Astron. Astrophys. 341, 751–767 (1999)

ASTRONOMY AND ASTROPHYSICS

Deep ROSAT HRI observations of the Pleiades⋆

G. Micela[1], S. Sciortino[1], F.R. Harnden Jr.[2], V. Kashyap[2], R. Rosner[3], C.F. Prosser[4,⋆⋆], F. Damiani[1], J. Stauffer[2], and J.-P. Caillault[5]

[1] Osservatorio Astronomico di Palermo, Palazzo dei Normanni, I-90134 Palermo, Italy
(e-mail: gmicela@oapa.astropa.unipa.it; ssciortino@oapa.astropa.unipa.it; fdamiani@oapa.astropa.unipa.it)
[2] Smithsonian Astrophysical Observatory-Center for Astrophysics, 60 Garden Street, Cambridge, MA 02138, USA
(e-mail: frh@cfa.harvard.edu; kashyap@cfa.harvard.edu; stauffer@cfa.harvard.edu)
[3] Department of Astronomy and Astrophysics and Enrico Fermi Institute, The University of Chicago, 5640 South Ellis Avenue, Chicago, IL 60637, USA (e-mail: rrosner@oddjob.uchicago.edu)
[4] NOAO, P.O. Box 26732, Tucson, AZ 85726-6732, USA
[5] Department of Physics and Astronomy, University of Georgia, Athens, GA 30602-24551, USA (e-mail: jpc@akbar.physast.uga.edu)

Received 23 June 1998 / Accepted 30 September 1998

Abstract. In a deep X-ray survey of the Pleiades open cluster, we use the ROSAT High Resolution Imager to explore a region of the cluster formerly surveyed with the PSPC. These new observations substantially improve upon both the sensitivity and the spatial resolution for this region of the Pleiades, allowing us to detect 18 cluster members not detected before and 16 members not included in the catalogs used in previous surveys. The high sensitivity of the present observations permits us to obtain more stringent upper limits for 72 additional members and also provides sufficient numbers of stars to enable us to explore the dependence of L_x on stellar rotation for the slow rotators of the Pleiades. Using the new high sensitivity X-ray observations and the recent rotational measurements we discuss the activity-rotation relationship in the Pleiades solar type stars.

We also present new photometric observations of optical counterparts of a number of X-ray sources detected in previous surveys but not yet identified.

Key words: X-rays: stars – stars: coronae – open clusters and associations: individual: Pleiades

1. Introduction

Observations of open clusters allow us to study the evolution of physical quantities during the main sequence life of stars. In the last few years, ROSAT observations have explored coronal properties in a large number of open clusters: Pleiades (Stauffer et al. 1994, hereafter Paper I, Schmitt et al. 1993, Gagné et al. 1995, Micela et al. 1996, hereafter Paper II), Hyades (Stern et al. 1992, 1994; Pye et al. 1994), IC 2391 (Patten & Simon 1993; 1996; Simon & Patten 1998), NGC 6475 (James & Jeffries 1997; Prosser et al. 1995a), IC 2602 (Randich et al. 1995), NGC 2516 (Dachs & Hummel 1996, Jeffries et al. 1997), Praesepe (Randich & Schmitt 1995), α Per (Randich et al. 1996a, Prosser et al. 1996, Prosser & Randich 1997, Prosser et al. 1997), Coma (Randich et al. 1996b), NGC 2422 (Barbera et al. in preparation), IC 4665 (Giampapa et al. 1998), NGC 752 (Belloni & Verbunt 1996), NGC 6940 (Belloni & Tagliaferri 1997) and IC 4651 (Belloni & Tagliaferri 1998). These observations have substantially increased our knowledge of the evolution of X-ray activity levels of late–type stars.

Notwithstanding this flourishing of new data, a number of issues remain unresolved. For example, the origin of the spread of the X-ray luminosity function (XLF) for open cluster members of a given spectral type is not understood: Thus, while it is known that this spread is smaller than the corresponding spread for field stars of the same spectral type, that the mean (and median) L_x decrease with age, and that fast rotators have activity levels higher than those of slow rotators, it is nevertheless unclear if the observed spread can be attributed simply to intrinsic variability of coronal emission. Furthermore, we do not understand how the evolution of X-ray luminosity depends on stellar mass, nor do we understand if and how this evolution is different for single and binary stars.

The Pleiades cluster represents a key sample of stars in any study of these issues: It is one of the best-studied open clusters, with a fairly complete membership list down to the mid-M dwarfs in the central region where our HRI fields are located, and has been the subject of an extensive campaign to measure rotational velocity and photometric periods (cf. Prosser et al. 1993a, 1993b, 1995b; Jones et al. 1996, Krishnamurthi et al. 1998, Queloz et al. 1998). Furthermore, its richness and proximity make it one of the best X-ray targets because it is possible to detect a significant fraction of the cluster stars with relatively small numbers of distinct pointings (in contrast to the Hyades, for example, in which the loose spatial distribution makes it quite time-consuming to obtain good coverage of its members). As a consequence, the Pleiades is the most deeply studied open cluster at X-ray wavelengths; since

Send offprint requests to: G. Micela
⋆ Table 2 is available in electronic form at CDS via ftp 130.79.128.5
⋆⋆ Deceased, Aug. 16, 1998

Table 1. Characteristics of the HRI observations: ROSAT observation Request (ROR) number, field center coordinates, nominal exposure times, dates of observation, and number of detections obtained using a Wavelet-based algorithm (cf. Sect. 2.1). For ROR 201412, we list separately two segments obtained nearly a year apart.

ROR	Field Name	R.A.(2000) h:m:s	DEC(2000) °:':"	Exposure Time [sec]	Start Date	End Date	Number of Detections
202069	H-A	3:42:21.6	24:55:48.0	30193	19-Feb-96	4-Mar-96	16
202070	H-B	3:43:14.3	25:16:12.0	29283	11-Feb-96	4-Mar-96	16
201412	H-1	3:44:14.3	24:06:00.0	4643	4-Sep-94	5-Sep-94	22
	H-1			22876	7-Aug-95	9-Aug-95	
201413	H-2	3:45:31.2	24:34:48.0	24202	13-Aug-94	22-Aug-94	29
201776	H-6	3:46:07.1	23:21:00.0	27846	20-Feb-95	24-Feb-95	20
202068	H-5	3:47:50.4	23:55.12.0	28896	21-Feb-96	4-Mar-96	35
201414	H-3	3:48:16.7	23:38:24.0	34160	5-Feb-95	6-Feb-95	36
202060	H-P	3:49:33.5	23:48:00.0	32629	9-Feb-96	2-Mar-96	24
						Total detections	--- 198

the launch of *Einstein*, X-ray survey observations have been reported by Caillault & Helfand (1985), Gagné et al. (1995), Micela et al. (1985, 1990, 1996), Schmitt et al. (1993), and Stauffer et al. (1994).

In order to explore some of the unresolved issues mentioned above, it is important to gain as complete a knowledge as possible of the X-ray emission properties of the Pleiades stars. As a further step in toward that goal, this paper reports and summarizes the full set of ROSAT HRI observations devoted to the investigation of this cluster.

Our paper is organized as follow: in Sect. 2 we describe the observations and data analysis and present data for the Pleiades stars; we discuss the relationship between the X-ray luminosity and rotation in Sect. 3 and summarize our results in Sect. 4. In the appendix A we present X-ray data for field stars, in appendix B, for sources not identified with cataloged objects together with new photometric observations of their optical counterparts. In the appendix C we present CCD photometry of cataloged stars around unidentified sources.

2. HRI observations and data analysis

We present data from eight ROSAT High Resolution Imager (HRI, Zombeck et al. 1990) observations targeted toward the Pleiades. These pointing directions were selected to resolve source-confused regions in images obtained with the ROSAT Position Sensitive Proportional Counter (PSPC, Briel & Pfeffermann 1995), and to narrow the error circles of previously unidentified PSPC sources. By targeting regions of the cluster previously covered only by the less sensitive external part of the PSPC field, these HRI exposures of about 30 ksec reached limiting sensitivities comparable (within a factor two) to those achieved in the central part of existing PSPC observations. In addition, one of the pointings (ROR 202060) was designed to determine the X-ray luminosities of HII-2341 and HII-2284, two of the mostly slowly rotating K dwarfs in the Pleiades.

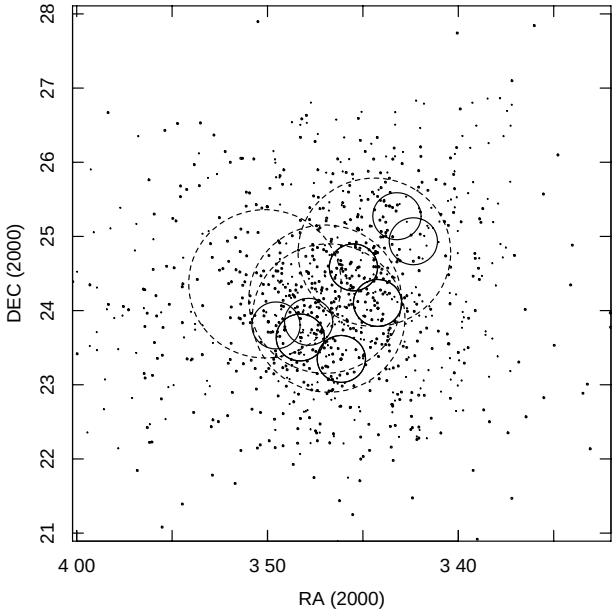

Fig. 1. Targeting of HRI (small solid circles) and previous PSPC (large dotted circles) observations, superposed on a map of known Pleiades stars.

A journal of observations is presented in Table 1. Note that the two segments of ROR 201412 were also analyzed separately since they were obtained nearly a year apart. For a subsample of stars, this circumstance and the partial overlaps between fields permit a study of X-ray variability on the time scale of a year.

In Fig. 1 we show the sky coverage of the HRI fields together with the optical positions of stars from the Pleiades membership catalog we have adopted.[1] Also indicated in the figure are the fields of view of previous PSPC observations (Paper I; Paper II).

[1] The Pleiades catalog employed in this study was provided by C. F. Prosser and J. R. Stauffer as part of the Open Cluster Database project, which currently may be accessed at http://cfa-www.harvard.edu/∼stauffer.

Note that the HRI fields targeted regions previously seen only in the outer, less sensitive regions of the PSPC fields of view.

The combined fields of view of the eight HRI images contain 260 stars with astrometric and/or photometric indications of membership; optical characteristics of these stars are summarized in Table 2. Photometry is photoelectric when such data are available, and photographic otherwise.

2.1. Source detections

For the detection of sources, we applied the Wavelet transform method of Damiani et al. (1997). While this algorithm does not require an exact knowledge of the detector point spread function (PSF), it was nevertheless specifically "tuned" for our HRI application (Damiani et al., in preparation). Over all fields, we found 177 distinct X-ray detections, some of which were detected in more than one field.

In this particular application of the algorithm, a flat fielded image was constructed from both an exposure map (which models the vignetted cosmic X-ray background and the intrinsic detector nonuniformities) and a particle map (which models particle-induced background that increases at large off-axis angles and contributes a substantial fraction of the total observed background, (Snowden 1998, Snowden et al. 1994).

Our detection thresholds were set to correspond roughly to a gaussian equivalent of 4.5 σ. For typical livetimes of $\sim$30 ksec, such thresholds yield $\sim$1 spurious source per field. Due to its high spatial resolution, the typical number of photons per HRI resolution element is small, even for rather long exposures. With photon statistics in the HRI images therefore far from the gaussian limit (cf. Damiani et al. 1997), a large number of simulations are required to determine proper acceptance thresholds. At the end of the detection process, we removed instrumental hot spots known to be present in a fraction of fields (cf. David et al. 1993).

Count rates were computed using source effective exposure time as function of position in the field of view (exposure map) computed according to the recipe of Snowden et al. (1994).

2.2. Identifications

Our search for catalogued counterparts of Pleiades X-ray detections used a coincidence circle of 20″ radius. Following the initial identification process, we deduced the presence of a systematic offset between the optical and X-ray positions of up to 6 arcsec (median of measured values in an individual image) in some of the observations. Such shifts are due to limitations of the ROSAT aspect corrections and are of the same order as the spatial resolution of the HRI. In order to improve our identifications, we corrected the X-ray source positions for the mean offset measured in each field and then repeated the identification process. After this second iteration, we identified 117 X-ray sources with 120 Pleiades members and 24 with field stars from SIMBAD catalogs or with stars known as non members, either from the Hertzsprung catalog (Hertzsprung 1947) or from HCG catalog (Stauffer et al. 1991). A remaining 36 detections could not be identified with any cataloged objects. An inspection of finding charts, reported in appendix B, shows that in a large fraction of the cases there is an "obvious" stellar counterpart inside the error circle. We identify most of the Pleiades stars with an offset smaller than 8 arcsec ($\sim$ 87%), all the other have an offset smaller than 15″ but one (HII-153[2]) that has an offset of $\sim$19 arcsec. In some cases a large offset can be due to position uncertainty in our optical catalog (such as in the case of TS-51x which has a position different by 8 arcsec from the corresponding star in the Guide Star Catalog, GSC). The probability of identifying an X-ray source with a Pleiades member uncorrelated with the emission is very small and the number of expected spurious identifications in the entire survey is less than 3.

Even the high angular resolution of the HRI was unable to resolve ambiguities in five cases: (1) HII-298/299, (2) HII-883/879, (3) HII-1794/1805, (4) HII-1392/1397, and (5) HII-2500/2507. For the purpose of computing luminosities, in the first three cases we apportioned the count rate equally between two late-type counterparts; in the remaining two cases, we attributed the emission to a late-type star rather than its A-type neighbor.

For purposes of consistency, we used the same Wavelet algorithm to determine count rate upper limits for all undetected members in our Pleiades catalog.

In seeking an explanation for the large number of unidentified sources, we computed the number of sources unrelated with the Pleiades expected in our fields, using sensitivity maps obtained from the Wavelet algorithm at a spatial resolution of $10'' \times 10''$. When a given area of sky was observed more than once, we retained the observation of highest sensitivity. For each $10'' \times 10''$ pixel we estimated the number of expected sources, assuming a hydrogen column $N_H = 10^{21}$ cm^{-2} obtained by interpolation from data of Stark et al. (1992) and power law spectra with photon indexes between 1 and 2. For our full 2.2 square degree region, we estimate a total of 26 to 27 field sources, using the log(N)-log(S) of Branduardi et al. (1994), or between 32 and 34 sources, if we adopt the log(N)-log(S) of Hasinger et al. (1993). These numbers suggest that most of our unidentified sources are of origin unrelated with the Pleiades.

2.3. X-ray fluxes and luminosities

We employed the detailed shape of the HRI PSF (David et al. 1993) in determining fluxes. We computed a conversion factor from count rate to flux in the 0.1–2.4 keV band, assuming a single-temperature Raymond spectrum with kT=0.8 keV and an average value of $\log N_H = 20.4$ cm^{-2}. Since Gagné et al. (1995) found typical Pleiades coronal temperatures in the range of 0.8–1.4 keV, our temperature assumption introduces a systematic conversion factor uncertainty of less than 20%. For stars with known anomalous reddening (Stauffer & Hartmann 1987), we have computed the conversion

[2] HII-153 is an A star and it is possible that it is not the true source of the emission

factors assuming kT=0.8 keV and the hydrogen column derived from the individual E(B-V). For consistency with previous X-ray measurements, luminosities were computed assuming the "standard" cluster distance of 127 pc instead of the new Hipparcos distance (116 pc, Mermilliod et al. 1997).

X-ray characteristics of the 260 Pleiades stars falling in our fields of view are summarized in Table 3, where the first and second columns list a running number and star name, and columns 3 and 4 report offsets between X-ray and optical positions in arc seconds of right ascension and declination, respectively. In column 5 we report the detection significance in equivalent σ (i.e., same probability as the normal distribution with this value). Columns 6 and 7 contain the X-ray count rate and its error, and columns 8 and 9, the value of L_x and L_x/L_{bol}, respectively. The bolometric correction has been computed using Johnson's (1966) data for stars with B - V < 1.34, Monet et al.'s (1992) data for stars redder than B - V > 1.34 or V - I > 1.6 and the conversion from M_V to M_{BOL} by Lang (1992) for the stars without measured colors. For B stars, the values of L_x and L_x/L_{bol} are placed in parenthesis because we believe they suffer UV leak contamination (cf. Sect. 2.4). We show in Figs. 2 and 3 scatter plots of L_x and $\log L_x/L_{bol}$ versus B - V, respectively. Vertical line segments connect different measurements for the same star. The distribution for HRI sources may be compared with the $\log(L_x/L_{bol})$ distribution based on PSPC sources in the Pleiades as shown by Giampapa et al. (1998, Fig. 5)

2.4. Indeterminate luminosities for B-type stars

An investigation of both the UV susceptibility of the HRI detector and the B-star count rates inferred in this study has led us to the conclusion that the HRI cannot determine accurate X-ray luminosities for B-type stars. Whereas the HRI detected 8 of 11 B stars present in the observed Pleiades region, the PSPC detected only 3 of these stars. Moreover, the HRI X-ray luminosities naively inferred for the three common B star detections are significantly higher than those measured with the PSPC.

Recent laboratory measurements have shown that the HRI UV/ion shield has a "UV leak" – enhanced transmission for wavelengths longward of $\sim$2000 Å(Barbera et al. 1997, Zombeck et al. 1997), where early-type stars with photospheric temperatures of the order of 10000-15000 K have the bulk of their emission. In spite of its much lower sensitivity to UV emission, however, the PSPC still detected some B stars. Hence we cannot arbitrarily attribute all detected HRI counts to UV contamination.

In Fig. 4 we report the measured luminosity excess (the difference between luminosity inferred from the HRI and that inferred from the PSPC) versus the absolute bolometric magnitude for the B stars in our survey. Also included in this figure is the excess for the star Vega (square+cross, from Zombeck et al. 1997), plotted by applying the conversion factor used here to its measured HRI count rate. The clear dependence of observed excess on absolute stellar magnitude is entirely attributable to the UV leak.

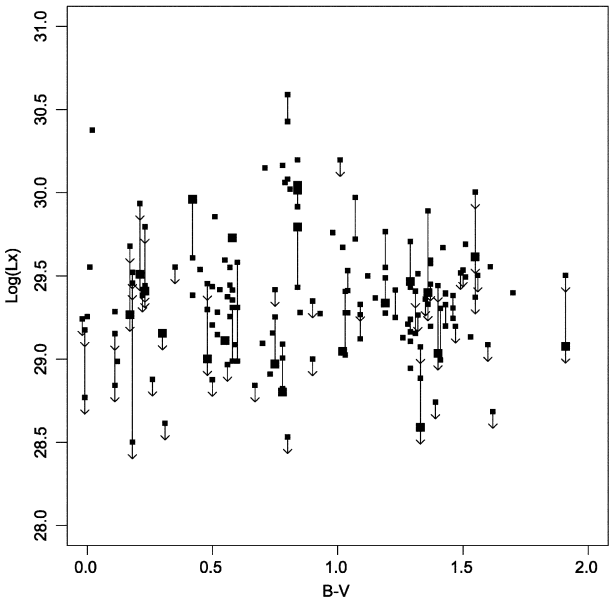

Fig. 2. Distribution of $\log L_x$ versus B - V. Vertical line segments connect different measurements of the same star.

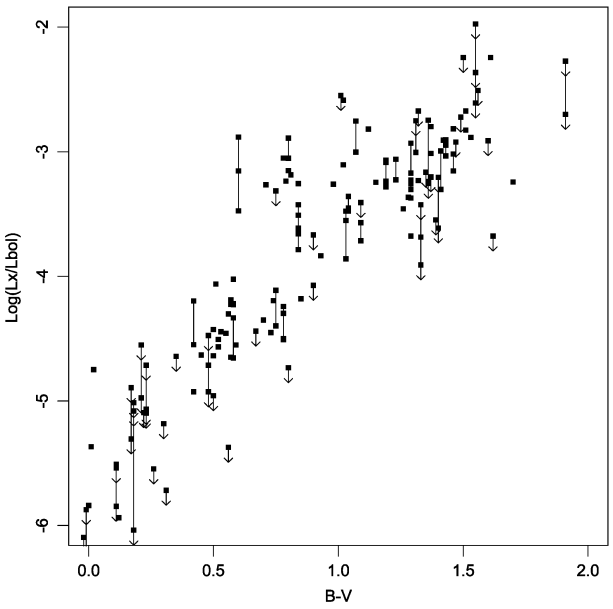

Fig. 3. Scatter plot of $\log(L_x/L_{bol})$ versus B - V. Vertical line segments connect different measurements of the same star.

3. X-ray emission and rotation

In this section we discuss the dependence of X-ray emission on rotation, concentrating mainly on the slow rotators. We take advantage of both newly available measurements of long periods and small rotations (Prosser et al. 1995b, Krishnamurthi et al. 1998, Queloz et al. 1998) and of the high sensitivity of the HRI observations (which allows us to detect faint sources).

In Fig. 5 we display the stellar X-ray luminosity (L_x) values obtained from the observations reported here versus the rotation rate for the corresponding stars, as measured by the projected

Table 3. X-Ray properties of observed Pleiades stars

#	Name	ΔRA [arcsec]	ΔDEC [arcsec]	S/N	Rate [cts/ksec]	±	$\log L_x$ erg/sec	$\log \frac{L_x}{L_{bol}}$	Field	off-axis [arcmin]
1	HHJ-126	...	...	...	<3.75	...	<29.39	<−2.12	H-A	18.1
2	HHJ-191	...	...	...	<3.26	...	<29.33	<−2.25	H-A	17.9
3	HHJ-148	...	...	...	<2.22	...	<29.16	<−2.00	H-A	16.3
4	HHJ-69	...	...	...	<0.89	...	<28.77	<−2.44	H-A	10.0
5	HHJ-125	...	...	...	<0.70	...	<28.66	<−2.76	H-A	9.1
6	HHJ-120	...	...	...	<2.05	...	<29.13	<−2.09	H-A	15.4
7	HCG-58	−8.1	5.3	8.3	7.15	1.71	29.67	−2.91	H-B	17.6
8	SK-702	1.6	3.1	5.6	0.74	0.25	28.69	−3.04	H-A	7.8
9	HHJ-212	...	...	...	<2.89	...	< 29.28	< −2.33	H-B	17.3
10	HCG-65	2.7	2.8	15.7	4.98	0.53	29.51	−3.23	H-A	13.7
11	HCG-71	1.2	−4.6	10.7	6.00	0.93	29.60	−2.80	H-A	15.9
12	AK-1b078	1.9	0.6	10.6	1.61	0.28	29.02	−3.86	H-A	7.2
13	SK-676	−0.1	2.7	10.5	1.53	0.27	29.00	−2.92	H-A	5.5
14	HCG-74	...	...	...	<0.51	...	< 28.52	< −2.66	H-A	6.8
15	HHJ-45	...	...	...	<0.67	...	< 28.64	< −2.51	H-B	8.5
16	HCG-93	...	...	...	<3.72	...	< 29.39	< −2.72	H-1	17.8
17	HHJ-107	...	...	...	<0.86	...	< 28.75	< −2.64	H-B	10.3
18	HCG-97	0.0	−0.9	9.1	1.87	0.50	29.09	−3.19	H-A	11.8
19	HCG-100	...	...	...	<4.87	...	< 29.50	< −2.51	H-A	17.9
20	SK-650	...	...	...	<0.82	...	< 28.73	< −2.94	H-B	9.2
21	HHJ-71	...	...	...	<1.72	...	< 29.05	< −2.21	H-1	14.4
22	HHJ-65	...	...	...	<1.42	...	< 28.97	< −2.21	H-1	13.3
23	HII-97	1.7	−2.4	12.4	3.94	0.58	29.41	−3.48	H-A	15.3
24	AK-1b121	−0.7	−0.30	45.2	17.56	0.93	30.06	−3.2	H-B	7.7
25	HCG-109	...	...	...	<1.92	...	< 29.10	< −2.61	H-A	15.2
26	HHJ-76	...	...	...	<1.00	...	< 28.82	< −2.31	H-1	10.9
27	HCG-112	...	...	...	<5.22	...	< 29.53	< −2.25	H-B	19.8
28	SK-622	...	...	...	<0.80	...	< 28.72	< −3.10	H-B	9.6
29	HII-134	−3.7	7.3	12.2	3.35	0.50	29.40	−3.24	H-1	11.8
30	HCG-115	−1.1	3.4	5.5	1.02	0.33	28.82	−3.11	H-B	9.8
31	HII-153	−18.5	4.9	10.8	2.94	0.48	29.28	−5.51	H-B	13.1
32	HII-158	...	...	...	<4.94	...	< 29.51	< −4.98	H-1	18.0
33	HHJ-43	...	...	...	<0.84	...	< 28.74	...	H-1	9.8
34	TS-51x	−11.0	−0.1	14.5	3.98	0.48	29.42	−4.44	H-B	11.4
35	SK-609	...	...	...	<1.90	...	< 29.10	< −3.29	H-B	15.0
36	HII-174	−2.1	4.8	15.7	16.08	3.38	30.02	−3.19	H-B	17.7
37	HII-173	2.9	−1.1	12.3	2.90	0.44	29.28	−4.18	H-B	9.1
38	HII-193	−0.8	2.8	8.3	1.42	0.43	28.97	−4.40	H-1	10.4
39	HHJ-218	...	...	...	<2.12	...	< 29.14	< −2.75	H-B	15.9
40	HCG-126	...	...	...	<1.86	...	< 29.09	< −2.91	H-B	15.2
41	SK-596	0.7	−1.2	6.2	1.14	0.35	28.87	−3.22	H-B	9.7
42	HCG-135	−1.7	−2.2	7.9	1.70	0.46	29.05	−2.59	H-1	9.7
43	HII-233	...	...	...	<1.53	...	< 29.00	< −4.93	H-1	13.5
44	JRS-26	...	...	...	<1.82	...	< 29.08	< −2.70	H-1	14.5
45	HCG-134	...	...	...	<2.39	...	< 29.20	< −2.92	H-B	16.4
46	HII-263	0.6	7.0	24.5	9.47	0.78	29.79	−3.43	H-1	10.8
47	AK-1b165	...	...	...	<2.67	...	< 29.24	< −3.68	H-B	17.2
48	SK-586	...	...	...	<6.81	...	< 29.65	< −2.11	H-2	18.6
49	AK-1b174	...	...	...	<1.78	...	< 29.07	< −4.03	H-B	15.1
50	HHJ-217	...	...	...	<1.47	...	< 28.98	< −2.67	H-1	13.4
51	HII-298	0.9	0.7	41.1	7.92	0.46	29.72	−3.81	H-1	4.1
52	HII-299	−4.6	3.8	41.1	7.92	0.46	29.72	−3.64	H-1	4.2
53	HII-303	−0.4	−0.8	39.9	16.85	0.97	30.04	−3.64	H-1	0.1
54	HCG-145	...	...	...	<4.09	...	< 29.43	< −2.46	H-2	18.5
55	HCG-146	...	...	...	<2.75	...	< 29.26	< −2.32	H-2	16.4
56	HII-320	−1.1	1.1	14.4	24.02	5.04	30.20	−3.26	H-2	19.9

Table 3. (continued)

#	Name	ΔRA [arcsec]	ΔDEC [arcsec]	S/N	Rate [cts/ksec]	±	$\log L_x$ erg/sec	$\log \frac{L_x}{L_{bol}}$	Field	off-axis [arcmin]
57	HHJ-57	...	...	...	<0.79	...	< 28.71	...	H-1	9.3
58	HII-324	...	...	...	<24.02	...	< 30.20	< −2.55	H-2	18.5
59	HII-335	1.0	0.7	13.8	3.31	0.41	29.34	−3.24	H-1	2.7
60	HCG-143	4.4	−10.3	5.4	5.47	1.53	29.56	−2.24	H-B	16.6
61	HII-338	0.4	0.9	36.6	13.92	0.95	29.96	−4.20	H-1	2.9
62	HCG-149	...	...	...	<24.02	...	< 30.20	< −1.98	H-2	18.9
63	HII-344	...	...	...	<3.91	...	< 29.41	< −5.10	H-1	17.9
64	HII-345	−3.4	0.6	31.4	18.44	1.13	30.08	−3.15	H-2	14.9
65	HHJ-243	...	...	...	<2.42	...	< 29.20	< −2.48	H-2	15.8
66	HCG-156	...	...	...	<3.59	...	< 29.37	< −2.61	H-2	17.9
67	HHJ-190	...	...	...	<0.74	...	< 28.68	< −2.80	H-1	8.8
68	HII-357	1.5	3.6	17.0	4.46	0.52	29.47	−3.17	H-1	5.3
69	HII-370	...	...	...	<1.65	...	< 29.03	< −3.61	H-1	14.0
70	HHJ-68	...	...	...	<5.76	...	< 29.58	< −1.74	H-B	19.3
71	HII-390	...	...	...	<0.59	...	< 28.59	< −3.91	H-1	7.6
72	HHJ-46	...	...	...	<2.2	...	< 29.16	< −1.99	H-2	15.2
73	HII-405	−7.7	−3.0	5.7	4.16	1.21	29.44	−4.43	H-2	18.4
74	HII-430	1.1	1.0	5.0	0.97	0.34	28.80	−4.50	H-1	10.4
75	HHJ-24	...	...	...	<2.43	...	< 29.20	...	H-2	15.6
76	HCG-166	...	...	...	<0.94	...	< 28.79	< −3.19	H-1	10.3
77	HII-447	3.4	5.9	6.3	1.81	0.53	(29.08)	(−6.79)	H-1	13.8
78	HII-470	...	...	...	<5.45	...	< 29.55	< −4.64	H-5	18.1
79	HII-468	3.6	−0.2	26.7	9.38	0.75	(29.79)	(−7.31)	H-1	8.7
80	HII-476	−5.6	−3.5	5.5	1.97	0.60	29.11	−4.46	H-1	14.0
81	HHJ-183	...	...	...	<1.35	...	< 28.95	< −2.57	H-2	11.6
82	HII-489	−3.7	−3.3	11.9	3.97	0.60	29.42	−4.22	H-2	11.9
83	HHJ-223	...	...	...	<2.54	...	< 29.22	< −2.41	H-6	16.3
84	HHJ-274	...	...	...	<1.78	...	< 29.07	< −2.69	H-1	14.4
85	HII-513	−9.6	−2.0	5.0	2.05	0.63	29.13	−3.46	H-6	15.8
86	HHJ-54	...	...	...	<2.20	...	< 29.16	< −2.07	H-6	15.6
87	HCG-172	...	...	...	<1.86	...	< 29.09	< −2.39	H-2	13.7
88	HII-522	...	...	...	<4.98	...	< 29.51	< −3.58	H-1	19.2
89	HHJ-48	...	...	...	<0.74	...	< 28.69	< −2.39	H-B	8.5
90	HII-531	...	...	...	<2.17	...	< 29.15	< −5.18	H-1	15.4
91	HII-541	...	...	...	<2.94	...	< 29.28	< −6.45	H-2	16.3
92	HII-554	−1.9	2.7	12.6	2.47	0.38	29.21	−3.37	H-2	4.4
93	HCG-177	...	...	...	<0.71	...	< 28.67	< −3.16	H-2	6.3
94	HCG-185	...	...	...	<1.37	...	< 28.96	< −2.59	H-6	12.7
95	HII-563	−0.9	−3.2	38.7	15.47	0.88	(30.01)	(−6.65)	H-2	8.0
96	HHJ-14	...	...	...	<3.29	...	< 29.33	...	H-1	18.0
97	HCG-183	...	...	...	<1.72	...	< 29.05	< −3.32	H-1	14.1
98	HCG-181	−3.5	−0.1	11.2	2.07	0.35	29.13	−2.88	H-2	3.4
99	HHJ-273	−2.3	3.3	5.4	0.89	0.30	28.77	−2.97	H-2	3.1
100	HII-636	...	...	...	<1.31	...	< 29.00	< −3.97	H-6	12.7
101	HII-624	...	...	...	<2.81	...	< 29.27	< −2.92	H-2	16.4
102	HII-652	...	...	...	<2.81	...	< 29.27	< −5.31	H-1	16.8
103	HHJ-99	...	...	...	<4.27	...	< 29.45	< −2.04	H-1	18.1
104	HHJ-106	...	...	...	<6.16	...	< 29.61	< −1.83	H-6	19.3
105	SK-520	...	...	...	<1.64	...	< 29.03	< −2.77	H-6	14.1
106	HII-673	...	...	...	<2.64	...	< 29.24	< −2.90	H-2	16.0
107	HII-686	−2.8	−12.1	5.8	3.82	1.08	29.40	−3.24	H-2	16.6
108	HII-697	...	...	...	<0.63	...	< 28.61	< −5.72	H-2	7.0
109	HII-708	1.5	−2.4	8.8	8.16	1.96	29.73	−4.02	H-1	18.8
110	HCG-194	−3.1	3.7	9.3	1.76	0.47	29.06	−2.95	H-2	4.5
111	HII-717	1.3	−4.0	4.6	1.48	0.50	28.99	−5.94	H-2	14.7
112	HII-727	-1.1	1.2	34.9	10.91	0.72	29.85	-4.06	H-2	3.5

Table 3. (continued)

#	Name	ΔRA [arcsec]	ΔDEC [arcsec]	S/N	Rate [cts/ksec]	±	$\log L_x$ erg/sec	$\log \frac{L_x}{L_{bol}}$	Field	off-axis [arcmin]
113	HII-745	2.1	0.3	5.3	3.03	0.92	29.30	−4.71	H-2	17.6
114	HII-746	−4.5	1.0	5.7	1.24	0.39	28.91	−4.45	H-2	9.2
115	HII-801	−1.9	4.1	11.6	2.75	0.45	29.26	−5.84	H-6	12.9
116	HII-785	−0.4	−5.0	12.4	5.86	0.78	(29.58)	(−7.41)	H-2	13.4
117	HHJ-25	...	...	...	<0.96	...	< 28.80	...	H-2	9.7
118	HCG-202	−2.3	4.8	8.9	1.39	0.38	28.96	−2.49	H-6	7.7
119	HII-813	...	...	...	<0.74	...	< 28.69	< −3.68	H-2	8.4
120	HII-817	6.7	0.3	9.7	2.00	0.37	(29.12)	(−6.54)	H-2	5.5
121	HII-859	...	...	...	<0.68	...	< 28.65	< −6.62	H-2	7.8
122	HII-882	−1.1	1.8	30.2	7.17	0.53	29.67	−3.11	H-6	3.4
123	SK-488	1.5	2.7	10.4	2.43	0.43	29.20	−2.87	H-2	8.1
124	HII-879	4.5	−3.2	9.6	1.45	0.26	28.98	−3.85	H-2	8.1
125	HII-883	−0.9	13.9	9.6	1.45	0.26	28.98	−3.75	H-2	8.2
126	HII-890	−5.8	−3.2	4.9	3.09	0.93	29.31	−2.82	H-2	14.8
127	HII-885	...	...	...	<6.69	...	< 29.64	< −3.42	H-2	19.1
128	HII-915	−2.0	3.2	15.5	2.88	0.37	29.28	−3.25	H-6	0.3
129	HII-906	1.1	1.9	15.9	4.76	0.58	29.49	−2.83	H-2	10.5
130	HII-923	−2.7	−0.0	23.8	5.42	0.51	29.55	−4.19	H-6	0.9
131	HII-916	3.6	−1.2	9.5	2.86	0.51	29.27	−3.84	H-2	9.6
132	HII-948	...	...	...	<1.41	...	< 28.97	< −5.37	H-6	13.3
133	HHJ-367	...	...	...	<1.53	...	< 29.00	< −3.13	H-2	12.4
134	HII-975	−1.1	1.9	12.0	1.87	0.32	29.26	−4.39	H-6	8.6
135	HII-974	...	...	...	<3.23	...	< 29.33	< −3.23	H-2	16.7
136	HHJ-33	...	...	...	<2.33	...	< 29.18	...	H-6	16.2
137	HHJ-105	...	...	...	<1.33	...	< 28.94	< −2.48	H-2	11.4
138	HII-996	4.5	−1.1	7.4	1.86	0.53	29.09	−4.55	H-2	11.7
139	HII-1005	...	...	...	<3.97	...	< 29.42	< −3.32	H-2	17.8
140	HHJ-249	...	...	...	<1.89	...	< 29.09	< −2.47	H-2	13.5
141	HHJ-326	...	...	...	<2.35	...	< 29.19	< −2.68	H-2	14.8
142	HII-1039	−1.3	5.2	13.3	5.66	0.74	29.76	−3.26	H-6	15.3
143	HII-1032	5.5	1.7	25.7	21.46	1.38	30.15	−3.27	H-2	15.7
144	HII-1029	...	...	...	<3.49	...	< 29.36	< −3.17	H-2	16.9
145	HII-1081	0.7	−0.3	11.3	1.65	0.28	29.11	−3.37	H-6	6.4
146	HII-1084	...	...	...	<2.81	...	< 29.47	< −5.06	H-6	17.6
147	HHJ-9	...	...	...	<0.57	...	< 28.57	...	H-B	7.5
148	HII-1103	2.2	1.7	11.7	2.10	0.35	29.20	−3.21	H-6	7.4
149	HHJ-140	...	...	...	<4.13	...	< 29.43	< −1.96	H-5	18.4
150	HII-1094	...	...	...	<3.26	...	< 29.33	< −3.26	H-5	17.3
151	SK-465	...	...	...	<5.21	...	< 29.53	< −1.97	H-6	18.0
152	HII-1117	...	...	...	<5.24	...	< 29.54	< −4.21	H-5	18.4
153	HII-1095	...	...	...	<4.68	...	< 29.49	< −3.67	H-2	18.2
154	HII-1110	...	...	...	<2.88	...	< 29.33	< −3.41	H-2	15.8
155	HII-1122	...	...	...	<7.48	...	< 29.69	< −4.38	H-5	19.7
156	HII-1124	...	...	...	<3.40	...	< 29.35	< −3.67	H-5	17.5
157	HII-1139	...	...	...	<2.29	...	< 29.18	< −4.86	H-6	16.2
158	HII-1136	2.3	2.0	38.5	16.47	0.89	30.16	−3.05	H-6	11.6
159	HHJ-104	...	...	...	<3.25	...	< 29.33	< −2.09	H-6	18.3
160	HHJ-75	...	...	...	<7.81	...	< 29.71	< −1.55	H-2	19.6
161	HHJ-159	...	...	...	<0.77	...	< 28.70	< −2.83	H-9	9.5
162	HII-1173	...	...	...	<5.04	...	< 29.52	< −2.72	H-2	17.8
163	HCG-240	−3.2	7.4	4.6	3.08	0.95	29.31	−2.07	H-6	14.7
164	HII-1200	...	...	...	<1.15	...	< 28.88	< −4.96	H-6	11.9
165	HII-1215	2.7	2.5	6.2	3.46	0.95	29.36	−4.23	H-6	17.6
166	HHJ-95	...	...	...	<0.95	...	< 28.80	< −2.49	H-5	11.2
167	HHJ-257	...	...	...	<1.34	...	< 28.94	< −2.59	H-5	12.6
168	HCG-247	-0.9	1.2	7.1	1.91	0.52	29.10	-3.08	H-6	12.8

Table 3. (continued)

#	Name	ΔRA [arcsec]	ΔDEC [arcsec]	S/N	Rate [cts/ksec]	±	$\log L_x$ erg/sec	$\log \frac{L_x}{L_{bol}}$	Field	off-axis [arcmin]
169	HHJ-174	...	...	...	<2.63	...	< 29.24	< −2.37	H-6	17.2
170	HHJ-299	...	...	...	<1.50	...	< 28.99	< −2.74	H-5	13.4
171	HII-1275	1.5	−3.6	6.1	1.55	0.47	29.01	−4.30	H-6	15.1
172	HII-1280	−11.9	−5.3	5.6	4.83	1.37	29.50	−2.82	H-5	17.9
173	HII-1286	...	...	...	<2.77	...	< 29.45	< −2.88	H-3	16.8
174	HII-1284	...	...	...	<1.15	...	< 28.88	< −5.55	H-5	11.5
175	HII-1298	...	...	...	<4.38	...	< 29.46	< −3.54	H-3	16.7
176	HII-1305	3.1	3.6	9.4	3.55	0.62	29.37	−3.25	H-6	15.6
177	HII-1306	−7.1	0.2	12.5	7.19	1.02	29.77	−3.07	H-5	15.8
178	HII-1321	−4.3	−2.6	9.5	3.80	0.64	29.40	−2.94	H-5	14.2
179	HII-1332	−4.2	9.1	7.3	2.81	0.73	29.27	−3.57	H-3	15.8
180	HCG-258	−2.4	1.0	11.6	2.18	0.38	29.16	−3.01	H-5	9.9
181	HHJ-203	...	...	...	<2.13	...	< 29.15	< −2.46	H-6	16.4
182	HII-1338	2.5	7.0	5.0	3.69	1.08	29.38	−4.93	H-5	14.7
183	HII-1355	0.8	3.0	13.6	3.60	0.47	29.43	−3.26	H-5	10.2
184	HII-1362	...	...	...	<3.69	...	< 29.38	< −5.09	H-5	15.0
185	HII-1380	...	...	...	<0.90	...	< 28.77	< −6.28	H-5	9.7
186	HII-1375	...	...	...	<2.66	...	< 29.24	< −6.09	H-5	13.6
187	HCG-266	0.7	3.8	4.7	0.86	0.30	28.75	−3.01	H-3	13.7
188	HII-1392	−2.2	−3.1	22.0	5.45	0.50	29.55	−4.12	H-5	6.1
189	HII-1397	...	...	...	<5.45	...	< 29.55	< −5.37	H-5	6.0
190	HHJ-427	8.1	−1.6	5.1	1.28	0.39	28.92	−3.23	H-5	9.7
191	HCG-269	0.5	4.9	5.2	1.30	0.39	28.93	−2.77	H-3	11.5
192	HII-1425	...	...	...	<1.06	...	< 28.84	< −5.85	H-3	11.7
193	SK-417	...	...	...	<2.30	...	< 29.18	< −2.62	H-3	16.0
194	HII-1432	1.1	5.3	33.2	13.80	0.82	(29.96)	(−7.63)	H-5	12.2
195	HHJ-16	...	...	...	<1.18	...	< 28.89	...	H-3	11.9
196	HCG-277	−2.3	3.0	14.1	3.24	0.43	29.33	−2.91	H-3	10.4
197	HHJ-73	...	...	...	<1.52	...	< 29.00	< −2.34	H-3	13.6
198	HII-1512	−4.2	0.9	5.1	1.34	0.43	28.94	−3.68	H-3	13.6
199	HII-1532	−1.0	3.5	13.6	2.71	0.34	29.25	−3.23	H-3	10.2
200	HII-1531	−1.0	3.1	23.0	5.74	0.51	29.58	−3.01	H-3	3.8
201	HHJ-26	...	...	...	<0.72	...	< 28.67	...	H-5	8.9
202	HHJ-152	−1.9	3.9	6.0	0.78	0.24	28.71	−2.88	H-3	8.2
203	HHJ-438	−1.7	5.5	7.6	0.93	0.29	28.79	−3.54	H-5	7.9
204	HHJ-122	...	...	...	<0.43	...	< 28.45	< −2.94	H-3	5.9
205	HII-1613	−0.1	3.3	13.4	2.44	0.35	29.20	−4.64	H-5	1.4
206	HII-1645	...	...	...	<1.06	...	< 28.84	< −4.44	H-3	11.6
207	HII-1695	...	...	...	<0.84	...	< 28.74	< −3.55	H-5	9.3
208	HHJ-21	...	...	...	<1.63	...	< 29.03	< −2.07	H-3	14.4
209	HHJ-240	−3.8	3.6	6.6	0.78	0.28	28.71	−2.92	H-5	6.1
210	HII-1726	5.0	2.8	11.9	6.00	0.81	29.60	−4.46	H-5	13.9
211	HCG-307	1.8	3.7	17.2	2.88	0.33	29.28	−2.17	H-3	6.3
212	HHJ-156	...	...	...	<0.43	...	< 28.45	< −3.09	H-3	4.4
213	HHJ-225	...	...	...	<0.48	...	< 28.50	< −3.16	H-5	5.5
214	HII-1756	−0.1	−1.6	7.9	1.17	0.33	28.88	−3.69	H-3	8.1
215	HCG-315	1.7	2.0	10.0	1.42	0.24	28.97	−2.66	H-3	0.8
216	HHJ-232	4.7	−3.4	9.7	2.64	0.45	29.24	−2.50	H-3	12.3
217	HHJ-336	3.2	1.2	6.9	0.92	0.28	28.78	−3.17	H-3	3.7
218	HHJ-151	...	...	...	<0.45	...	< 28.47	< −2.95	H-3	3.1
219	HII-1797	1.5	1.1	11.9	2.13	0.35	29.15	−4.57	H-3	0.2
220	HII-1794	2.9	1.3	14.5	1.56	0.20	29.01	−4.64	H-5	6.3
221	HHJ-188	...	...	...	<0.79	...	< 28.71	< −2.82	H-5	9.2
222	HII-1805	−11.7	−1.2	14.5	1.56	0.20	29.01	−3.45	H-3	6.5
223	HCG-321	...	...	...	<0.53	...	< 28.54	< −2.21	H-3	7.3
224	HII-1823	2.9	−0.9	5.0	0.93	0.30	(28.78)	(−7.09)	H-3	13.1

Table 3. (continued)

#	Name	ΔRA [arcsec]	ΔDEC [arcsec]	S/N	Rate [cts/ksec]	±	logL_x erg/sec	log$\frac{L_x}{L_{bol}}$	Field	off-axis [arcmin]
225	HHJ-171	...	...	...	<0.96	...	< 28.80	< -2.71	H-3	10.8
226	HII-1827	3.1	3.3	14.4	2.68	0.38	29.25	-3.16	H-5	8.0
227	HII-1856	4.6	4.7	9.5	2.91	0.51	29.28	-4.51	H-5	11.2
228	HCG-328	...	...	...	<0.84	...	< 28.74	< -2.60	H-5	9.4
229	HHJ-184	...	...	...	<1.25	...	< 28.91	< -2.67	H-5	12.0
230	HII-1924	4.5	-4.3	12.6	4.25	0.63	29.44	-4.23	H-3	12.9
231	HII-1912	1.6	6.6	5.6	5.27	1.44	29.54	-4.63	H-5	18.7
232	HCG-335	...	...	...	<6.03	...	< 29.60	< -1.65	H-5	19.7
233	HHJ-96	...	...	...	<6.00	...	< 29.60	< -1.56	H-5	19.7
234	HHJ-207	...	...	...	<5.57	...	< 29.56	< -2.07	H-5	19.7
235	HHJ-86	...	...	...	<1.92	...	< 29.10	< -2.11	H-3	15.4
236	HII-2034	1.4	0.9	31.0	14.31	0.85	29.97	-2.75	H-5	13.9
237	HII-2144	-1.7	-0.6	12.3	3.8	0.45	29.30	-2.99	H-P	7.3
238	HII-2147	6.4	3.1	65.2	40.96	1.29	30.43	-3.05	H-3	14.1
239	HII-2168	2.1	4.4	13.7	7.21	1.55	(29.67)	(-7.46)	H-P	16.2
240	HII-2193	2.1	-1.3	9.3	2.64	0.48	29.24	-3.23	H-P	15.5
241	HII-2195	...	...	...	<0.48	...	< 28.50	< -6.04	H-P	7.2
242	HCG-362	5.9	8.1	6.1	2.15	0.61	29.15	-3.24	H-P	16.3
243	HHJ-308	...	...	...	<1.38	...	< 28.96	< -2.65	H-P	13.6
244	HCG-363	-1.4	-6.6	4.7	0.81	0.28	28.73	-3.03	H-P	9.3
245	HII-2281	...	...	...	<0.41	...	< 28.43	< -3.97	H-P	5.4
246	HII-2284	1.5	1.0	10.8	2.19	0.37	29.16	-4.20	H-P	3.3
247	HII-2311	5.0	-6.7	5.9	1.01	0.32	28.82	-4.51	H-P	5.4
248	HHJ-158	...	...	...	<0.75	...	< 28.69	< -2.87	H-P	9.1
249	HHJ-142	-1.3	-1.2	6.3	1.12	0.33	28.87	-2.62	H-P	6.7
250	HII-2341	7.5	-1.1	7.7	1.89	0.38	29.09	-4.35	H-P	0.3
251	HII-2425	...	...	...	<0.50	...	< 28.51	< -6.89	H-P	5.7
252	HII-2462	...	...	...	<0.52	...	< 28.53	< -4.73	H-P	6.8
253	HII-2500	2.6	0.3	68.2	18.12	0.62	30.08	-3.40	H-P	6.1
254	HII-2507	...	...	...	<36.24	...	< 30.38	< -4.75	H-P	6.3
255	SK-293	0.2	-1.5	12.9	2.71	0.38	29.25	-2.74	H-P	7.8
256	HHJ-256	...	...	...	<1.17	...	< 28.88	< -2.93	H-P	12.6
257	HII-2602	5.7	2.2	13.7	6.43	0.75	29.69	-2.67	H-P	14.7
258	HII-2655	...	...	...	<2.80	...	< 29.26	< -2.67	H-P	17.3
259	HCG-396	...	...	...	<1.44	...	< 28.97	< -2.19	H-P	14.1
260	HII-2786	3.9	2.8	5.0	3.61	1.02	29.37	-4.30	H-P	17.1

equatorial rotation rate ($v\ \sin(i)$) for G stars, defined as stars with 0.5 ≤ B-V_0 < 0.8 (Fig. 5a) and K stars, defined as 0.8 ≤ B-V_0 <1.4 (Fig. 5b); vertical line segments connect different measurements of the same star. Filled symbols represent stars with $B\ -\ V \leq 0.63$ and $B\ -\ V \leq 1.1$, in the two panels, respectively.

These two figure panels suggest that G and K stars in the Pleiades are in two different regimes as far as concern the rotation-coronal emission connection: Whereas the G star sample displays a correlation between L_x and $v\ \sin(i)$ (albeit with a best-fit regression slope less steep than that of the canonical "Pallavicini law," $L_x \propto v^2$), the Pleiades K star sample does not show such a correlation between X-ray luminosity and rotation, down to values of $v\ \sin(i) \sim 3\,\mathrm{km\,s^{-1}}$. Furthermore, whereas the G stars show a scatter about the best-fit regression curve of roughly half an order of magnitude, the spread of X-ray luminosities for K stars is larger than one order of magnitude. Moreover, we note that in both cases, the Hyades member stars (pluses) tend to cluster in a region of these diagrams lying below the distribution of Pleiades data points. We also note that if we use L_x/L_{bol} as an activity indicator, instead of L_x, the weak dependence on rotation seen in the Pleiades G star sample disappears altogether; this effect may simply reflect the fact that the Pleiades G stars with the bluest color (and largest values of L_{bol}) tend to have systematically higher rotational velocities, concentrated in the 10-20 km s^{-1} range, with very few stars with $v\ \sin(i) \leq 5\,\mathrm{km\,s^{-1}}$. Finally, it is striking that for the K star sample, the use of L_x/L_{bol} as an activity indicator, rather than L_x, reduces the observed scatter; however, in this case it is also true that ∼ half of the slow rotators have the same activity levels (as measured by L_x/L_{bol}) as the fast rotators.

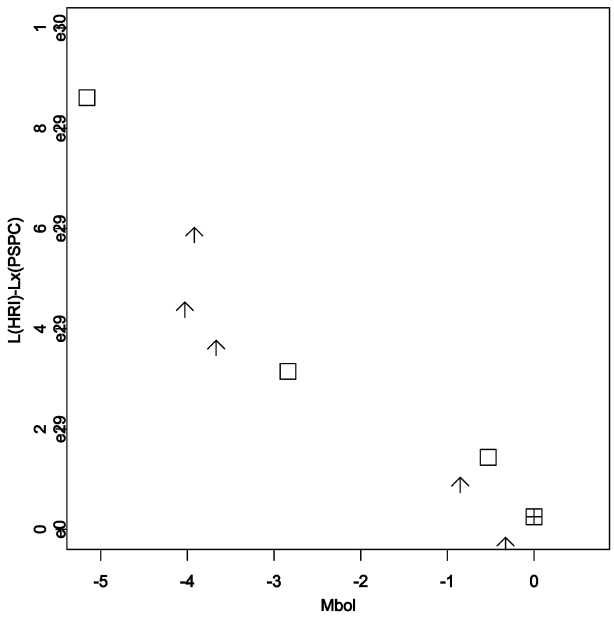

Fig. 4. Measured luminosity excess (difference between luminosities inferred from the HRI and the PSPC) versus absolute bolometric magnitude for B stars in our survey. Open squares indicate the three stars detected both in the HRI and PSPC, the arrows indicate the stars detected with the HRI and undetected with the PSPC. The square with plus indicate Vega (see text).

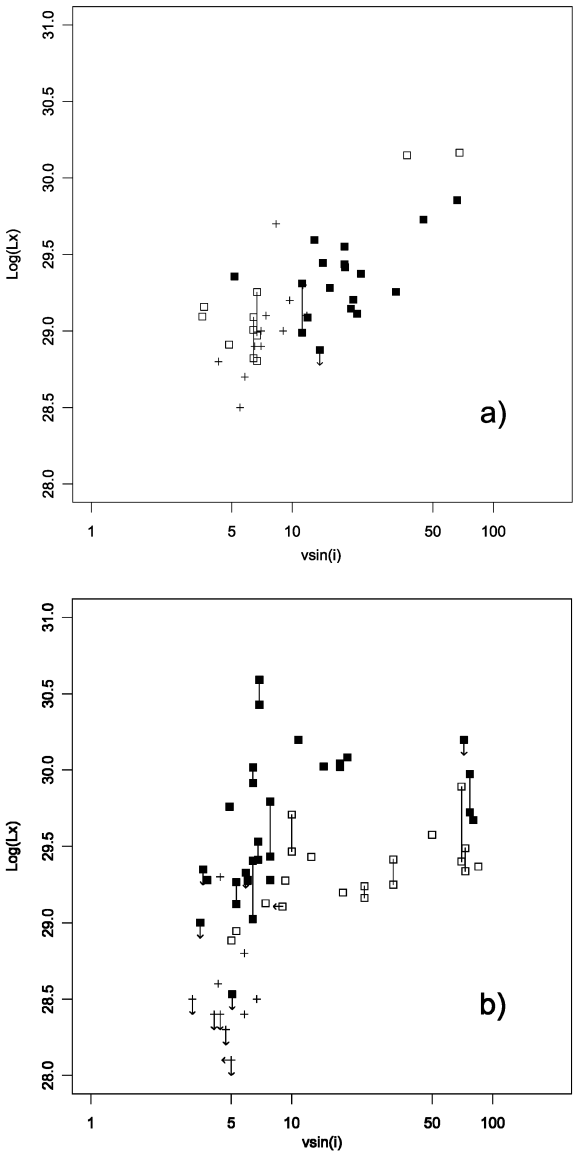

Fig. 5a and b. Scatter plot of L_x vs. $v\ sin(i)$ for stars with $0.5 \leq$ B - $V_0 < 0.8$ (panel **a**) and with $0.8 \leq$B - $V_0 < 1.4$ (panel **b**). Vertical line segments connect different measurements of the same star. Plus-sign points represent the Hyades. Filled symbols in panel **a**) represent stars with B - $V_0 < 0.63$. Filled symbols in panel **b** represent stars with B - $V_0 < 1.1$.

The usual explanation for these observations relies upon the properties of a star that determine the control parameters of linear dynamo theory, i.e., the depth of the convection zone, the convective turn-over time scale τ_{conv}, and the Rossby number (the ratio between the stellar rotational period and the convective time scale; see Noyes et al. 1984). These arguments have however severely flawed precisely because they are based entirely on reasoning developed from linear dynamo theory: Linear dynamo theory predicts the rate of growth of unstable magnetic dynamo solutions, but cannot be used to predict the nonlinear behavior of these solutions; in contrast, observed stellar magnetic activity (and whence stellar magnetic dynamos) are observed in a manifestly nonlinear state (since stellar magnetic fields are not observed to grow at exponential rates). Since the nonlinear mechanisms which are thought to limit the growth of stellar magnetic fields are entirely different from those processes which lead to the instability in the first place, it would be remarkable if the nonlinearly-determined amplitudes depended on the control parameters of the linear problem.

It might therefore be useful to consider anew the process of nonlinearly-limited dynamo growth and the associated limitations on stellar activity, and quite apart from the linear problem. As a starting point, we note that the dynamo process can be viewed as a heat engine which produces magnetic fields as a consequence of being (ultimately) powered by a star's nuclear burning. Since stellar dynamos operate in a nonlinearly-limited regime, correlating the work done by these heat engines with stellar properties (such as mass and rotation rate) requires one to compute properties of stellar activity averaged over time scales long when compared to their activity cycles. In that way, one can (for example) compute the statistically-steady quantity of magnetic flux (or the associated X-ray activity level) generated by the dynamo process; these statistically steady indicators of stellar activity are then a measure of the thermodynamic efficiency of the dynamo engine.

Now, let us focus on stars of a given mass. In that case, the observations tell us that as such stars age, they despin, and that as they despin, we observe a steadily-decreasing X-ray luminosity and L_x/L_{bol} ratio. Hence, we can conclude that the dynamo's thermodynamic efficiency declines with stellar rotation. This simple-minded picture has a definite prediction for the

expected scaling of L_x on stellar rotation for a stellar population of fixed age (as in clusters): the corresponding scaling exponent should be smaller than that obtained for a stellar population of fixed mass but broad distribution in stellar age (and hence in stellar rotation rate). This point is consistent with the results of Pallavicini et al. (1981), which showed a relationship between $v\ \sin(i)$ and L_x, but not with L_x/L_{bol}, for slowly–rotating stars of various spectral types.

What about "saturation" of stellar activity? Whatever the precise nature of the saturation process, one expects it to be fundamentally related to the backreaction of the magnetic Lorentz force on the internal motions of the star which gives rise to the dynamo effect. Model calculations of nonlinear dynamos (e.g., Cattaneo & Hughes 1996; Vainshtein, et al., 1997) show that when dynamos attain nonlinear saturation (not to be confused with the "activity saturation" just mentioned above), the total magnetic energy tends to a maximal statistically-steady value, so that the total magnetic flux produced tends to a statistically-steady maximal value. This maximal value is associated with a maximal field strength, and a magnetic field filling factor whose value depends upon the control parameters of the calculation. We now conjecture that stellar rotation largely determines this filling factor, and not the maximal field strength. In that case, one can associate "activity saturation" with saturation of the filling factor; that is, we conjecture that there is a maximal value of the magnetic field filling factor, which we will identify with the maximal magnetic flux state found, for example, in the surface magnetic flux distribution in solar active regions. The activity–saturated state should then correspond to covering the entire stellar surface with activity similar to solar active region levels. This picture has several implications: First, it implies that for "activity saturated" stars, L_x should vary with stellar mass for the simple reason that stars with smaller mass have smaller surface area; this is observed. Second, it implies that "activity–saturated" stars should show a very weak, if any, variation in the L_x/L_{bol} ratio (since both decline with stellar mass); this is observed. Third, this simple model predicts that "activity–saturated" stars should have mean surface X-ray fluxes at solar active region levels (i.e., $\sim 10^7$ ergs cm^{-2} s^{-1}); this is also observed.

More specifically, we can ask to what extent the observations support the implications of this theoretical model picture. As already mentioned, Pallavicini et al. (1981) demonstrated a relationship between $v\ \sin(i)$ and L_x, but not with L_x/L_{bol}, for slowly–rotating stars of various spectral types; this is expected on the basis of the just–discussed model. Furthermore, for stars with X-ray luminosities sufficiently large that $\log L_x/L_{bol} \simeq -3$, the data suggests that such stars then enter a "saturated" regime, where no further increases in X-ray production are observed (Stauffer et al. 1994). In this regime, L_x is determined by L_{bol}, and not any longer by rotation; again, this is as expected in our model. Panel (b) of Fig. 5 illustrates this effect: it shows that the "saturated" bluest stars (filled symbols) lie systematically above the comparable reddest stars. Thus, one would expect – and one sees – that in the $L_x - v\ \sin(i)$-plane, stars of different spectral types occupy the same position if they

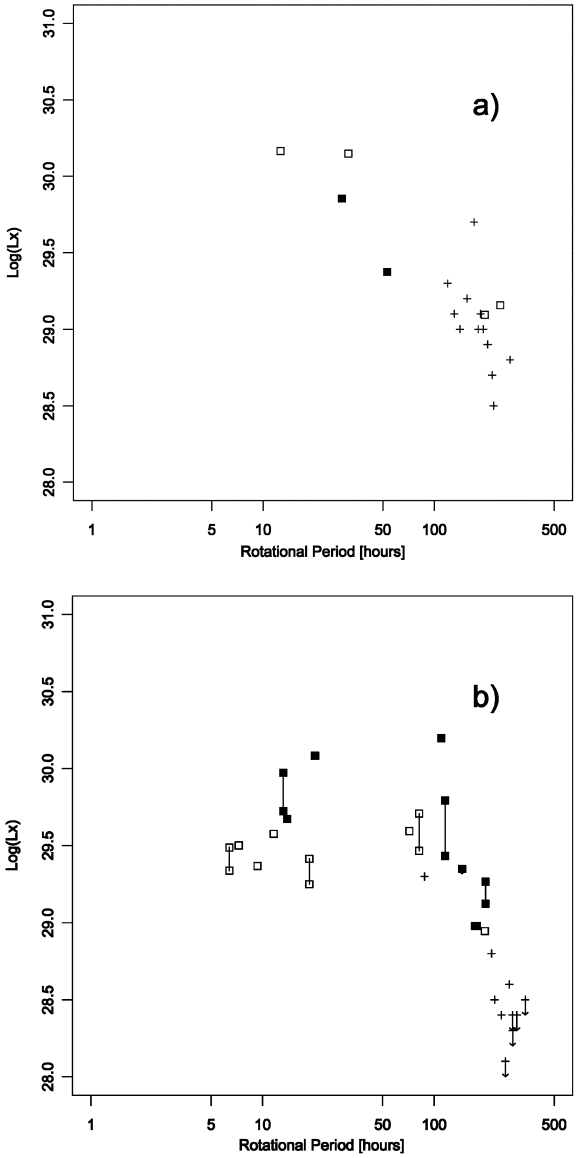

Fig. 6a and b. Scatter plot of L_x vs. rotational period for G (panel **a**) and K stars (panel **b**). Symbols as in previous figure.

are slow rotators, while in the activity–saturated regime stars occupy different regions which are arranged in parallel horizontal lines, each corresponding to a fixed value of the L_x—L_{bol} ratio; a similar (but cleaner) picture is expected if one can measure the stellar rotation period instead; indeed, we display in Fig. 6 a scatter plot of X-ray luminosity (L_x) versus rotational *period* for a subset of Pleiades stars for which the rotational period could be obtained independently from measurement of the projected equatorial rotation speed. This figure, although based on a much smaller sample size, nevertheless is consistent with the notion that the dwarf K star slow rotators of the Pleiades are already in an "activity–saturated" regime. In this figure, the Hyades have periods longer than those of analogous stars in the Pleiades, and appear to be far away from the saturated regime.

An interesting question is at what value of the stellar rotation rate the transition to "activity saturation" takes place, and how

Table A1. X-ray detections of field stars or of stars with unknown membership

Name	R.A. (J2000)	Dec. (J2000)	ΔRA [arcsec]	ΔDEC [arcsec]	V	B-V	V-I_K	S/N	Rate [cts/ksec]	±	Field	Offaxis [arcmin]	Memb.
HCG-50	3:41:33.59	25:06:49.8	6.8	3.9	17.25	...	2.14	4.8	2.40	0.74	H-A	15.6	N
HCG-102	3:43:12.02	24:44:46.7	−3.1	−12.9	17.16	...	2.85	4.6	4.70	1.42	H-A	15.9	N
HII-52	3:43:13.4	25:16:01.	1.5	13.5	13.02	...	...	31.8	9.02	0.63	H-B	10.2	
HII-180/182	3:43:47.7	24:02:20.0	4.5	1.7	12.01/16.0	...	...	7.8	1.63	0.46	H-1	7.1	
AK-1B146	3:43:50.51	25:16:09.5	3.4	−0.3	9.63	0.52	...	4.9	0.63	0.23	H-B	8.3	N
HCG-133	3:43:57.18	24:13:21.6	1.9	3.5	17.57	...	2.44	5.6	1.09	0.36	H-1	8.3	N
HCG-140	3:44:09.87	24:16:06.1	0.7	−1.0	16.20	...	2.17	7.4	1.55	0.44	H-1	10.2	N
HCG-160	3:44:39.50	24:31:44.2	0.0	−3.7	16.79	...	2.53	6.8	2.13	0.60	H-2	12.2	N
HCG-173	3:44:57.02	23:59:30.8	10.5	4.0	14.53	...	1.08	7.9	2.16	0.58	H-1	11.7	N
HD 23353	3:45:22.57	23:12:17.5	2.6	0.4	8.6	...	...	9.3	2.60	0.48	H-6	13.6	
HII-659	3:45:25.86	23:25:49.6	−3.6	2.9	12.04	0.94	0.94	17.8	4.59	0.50	H-6	10.6	N
HCG-225	3:46:31.97	23:59:00.5	−3.2	9.2	14.55	...	...	5.9	4.88	1.34	H-5	18.3	N
HII-1403	3:47:24.1	23:54:03.3	7.7	−4.6	14.62	...	...	4.7	0.65	0.24	H-5	6.1	
HII-1576	3:47:47.5	23:54:28.9	0.0	1.9	14.4	...	...	6.4	0.94	0.29	H-5	0.8	
HII-1644	3:47:55.8	23:40:00.0	6.0	15.6	16.2	...	...	4.6	0.41	0.18	H-3	5.5	
HCG-303	3:47:58.89	23:29:07.8	−0.3	−2.7	16.75	...	3.24	11.5	2.20	0.34	H-3	10.1	N
HCG-310	3:48:11.10	23:39:44.8	1.8	2.8	16.49	...	2.27	6.1	0.79	0.25	H-3	1.9	N
HCG-311	3:48:13.20	23:58:48.4	2.4	2.5	17.81	1.04	2.90	8.0	1.29	0.34	H-5	6.3	N
HII-1857	3:48:25.1	23:38:11.3	4.6	2.7	12.38	...	...	5.1	0.50	0.17	H-3	2.2	
HCG-326	3:48:31.66	24:04:44.8	7.9	10.8	18.00	...	...	4.5	1.60	0.53	H-5	13.4	
HD 23822	3:48:56.9	23:51:28.8	15.0	0.6	6.47	0.42	...	6.9	1.60	0.44	H-P	9.8	
HII-2296	3:49:25.6	23:48:32.9	4.6	2.9	12.55	...	...	6.2	0.81	0.25	H-P	2.0	
HCG-373	3:49:35.99	23:56:24.7	0.7	−0.7	17.42	...	2.26	6.9	1.66	0.46	H-P	8.4	N
HD 283068	3:49:58	23:57.3	7.5	5.6	9.4	...	...	7.2	1.77	0.48	H-P	11.0	

this value depends on the value of L_{bol}. The data in hand provides a hint as to when saturation occurs: the transition occurs when $L_x/L_{bol} \simeq$-3 i.e. when $\log(L_x) \simeq A + B*\log(v\ sin(i)) \simeq \log(L_{bol})$ - 3. This determines the rotation at which the transition occurs for a given L_{bol}.

4. Summary

We have presented the results of a deep ROSAT HRI survey of the Pleiades region. The high sensitivity of these HRI observations allows us to detect 18 Pleiades stars below the threshold of the previous PSPC observations and 16 stars not included in the region of previous surveys. Most of this latter group are low–mass stars. In addition, we have further constrained previous upper limits for 13 other members of this open cluster and report new X-ray upper limits for 72 optically-catalogued stars.

We confirm the existence of 10 X-ray sources with prior PSPC detections but no optical identification, and we report the discovery of 26 new X-ray sources whose optical counterparts are as yet unknown. A significant fraction of this latter group of sources is likely of extragalactic origin.

New photometric observations of optical counterparts of X-ray sources not identified with known cataloged stars have been presented.

Our results show that the dwarf G and dwarf K stars in the Pleiades are in two different activity regimes: First, the G stars show a L_x–$v\ sin(i)$ correlation (similar, but not identical, to the "Pallavicini law"), but the K stars do not; second, the spread of X-ray luminosities for the K stars is larger than for the G stars. Our results thus confirm that the K stars in the Pleiades are in a "saturated" regime as far as rotation–activity correlation is concerned.

Acknowledgements. This paper is dedicated to the memory of Charles Prosser, whose hard work and dedication to astronomy were unmatched and whose companionship we will miss. GM, FD and SS acknowledge financial support from ASI (Italian Space Agency), and MURST (Ministero della Università e della Ricerca Scientifica e Tecnologica). FRH and RR acknowledge support by NASA grants to the Smithsonian Astrophysical Observatory (NAG5-2644; NAG5-4967) and the University of Chicago, respectively. JS acknowledges support from NASA grant NAGW-2698. CP acknowledges support by a NASA grant to the Smithsonian Astrophysical Observatory (NAG5 -2203). We thank D. Queloz that provided us his rotational data before publication.

Appendix A: field stars

We have identified 24 X-ray sources with field stars or with stars of unknown membership status present in other catalogs. For these sources we report X-ray data in Table A1, where the columns have the same meanings as corresponding columns of Tables 2 and 3. We do not include in this table the three X-ray sources identified with solely GSC cataloged stars, for which no other information is available.

Table B1. Unidentified X-ray sources. PLHX is a running number indicating unidentified source in present HRI X-ray survey. PLEX number are from Stauffer et al. (1994)

# PLHX	RA (J2000)	DEC (J2000)	S/N	Rate (cts/ksec)	±	Notes	Field	Offaxis [arcmin]
1	3:41:25.7	24:46:43.7	4.7	1.89	0.61		H-A	15.7
2	3:42:01.7	25:06:59.2	7.4	1.93	0.51	GSC	H-A	12.1
3	3:42:12.5	24:52:46.8	7.8	1.15	0.33		H-A	3.7
4	3:42:14.2	24:59:26.8	21.1	3.98	0.39	PLEX3	H-A	4.0
5	3:42:22.3	24:56:01.8	9.6	1.54	0.29	PLEX5	H-A	0.3
6	3:42:42.4	25:16:51.9	5.4	0.56	0.19	GSC	H-B	7.3
7	3:42:47.0	25:09:01.9	7.8	2.10	0.55		H-B	9.5
8	3:43:13.3	24:52:48.8	6.5	1.66	0.48	PLEX14	H-A	12.2
9	3:43:16.7	24:54:08.7	4.8	1.20	0.39	PLEX15	H-A	12.7
10	3:43:25.4	24:08:34.7	7.0	1.90	0.54		H-1	11.5
11	3:43:39.5	25:16:49.4	12.8	2.19	0.32		H-B	5.8
12	3:44:27.3	24:04:45.1	5.0	0.53	0.21		H-1	3.2
13	3:44:36.2	24:19:10.1	5.4	1.46	0.48	GSC	H-1	14.1
14	3:44:49.5	24:04:04.9	4.9	0.52	0.21		H-1	8.2
15	3:45:00.5	24:37:20.9	5.8	1.26	0.41	PLEX78	H-2	7.5
16	3:45:09.4	24:27:56.0	4.6	0.58	0.23		H-2	8.5
17	3:45:15.4	24:40:13.5	9.0	1.49	0.29	PLEX87	H-2	6.5
18	3:45:17.1	24:27:06.0	7.8	1.45	0.39		H-2	8.3
19	3:45:19.6	24:28:26.0	13.9	3.44	0.51		H-2	6.9
20	3:45:49.8	23:16:25.4	4.7	0.49	0.21		H-6	6.1
21	3:46:26.8	23:07:50.3	4.8	1.66	0.54		H-6	13.9
22	3:47:08.9	24:03:15.6	7.7	2.14	0.57	PLEX166	H-5	12.4
23	3:47:30.7	23:36:22.2	4.9	1.62	0.49		H-3	10.7
24	3:47:37.4	23:55:43.4	4.6	0.62	0.23		H-5	3.0
25	3:47:39.2	23:33:59.8	14.1	3.15	0.41	Paper II (tab.6)	H-3	9.6
26	3:47:57.2	23:39:57.5	7.4	0.77	0.24		H-3	4.7
27	3:48:11.0	23:32:35.1	4.8	0.62	0.21		H-3	6.0
28	3:48:11.3	23:45:00.9	4.6	4.39	1.31		H-5	11.3
29	3:48:19.8	23:36:12.6	8.8	0.99	0.28		H-3	2.3
30	3:48:21.0	23:52:58.3	15.6	3.16	0.39		H-5	7.3
31	3:48:28.1	23:55:05.7	5.0	0.93	0.31		H-5	8.6
32	3:48:32.9	23:28:57.6	4.5	0.59	0.21		H-3	10.1
33	3:48:41.2	23:32:37.5	8.3	11.43	2.05	Ext. PLEX313	H-3	8.0
34	3:49:07.1	23:35:17.1	4.9	1.16	0.37		H-3	11.9
35	3:49:13.7	23:46:17.0	4.9	1.64	0.50		H-3	15.2
36	3:50:00.4	23:33:48.7	16.3	6.82	0.72	PLEX314	H-P	15.5

Using the model "X-Count" of Favata et al. (1992) modified to take into account the dependence of stellar emission level on age (cf. Micela et al. 1993 and Sciortino et al. 1995), we expect to detect $\sim$10 field stars in the combined HRI fields of view, about one third of the overall number of sources (galactic and extragalactic) expected on the basis of log(N)-log(S) of Hasinger et al. (1993) or Branduardi et al. (1994). Since the number of detections we attribute to field stars lies about 3σ above this expectation, it is possible that a small number of our "field stars" are actually cluster members or members of the nearby Taurus association.

Appendix B: sources unidentified with cataloged stars

The characteristics of the remaining 36 sources with no known counterparts are reported in Table B1. Some of these sources were previously detected with the PSPC (Paper I and Paper II), as indicated. Three stars, with possible GSC identifications are included in this table. The unidentified sources are of special interest because in principle some may be unknown cluster members, other field stars or perhaps stars belonging to the adjacent Taurus star forming region or the Hyades cluster. Given the high number of expected extragalactic sources and the faintness of plausible counterparts in the POSS plates, however, it is perhaps more likely that most of these sources are of an extragalactic nature.

In Fig. B1 we present finding charts from Digitized Sky Survey centered on the positions of the remaining unidentified sources. The 20″ arcsec radius identification circle we have used is indicated on the charts.

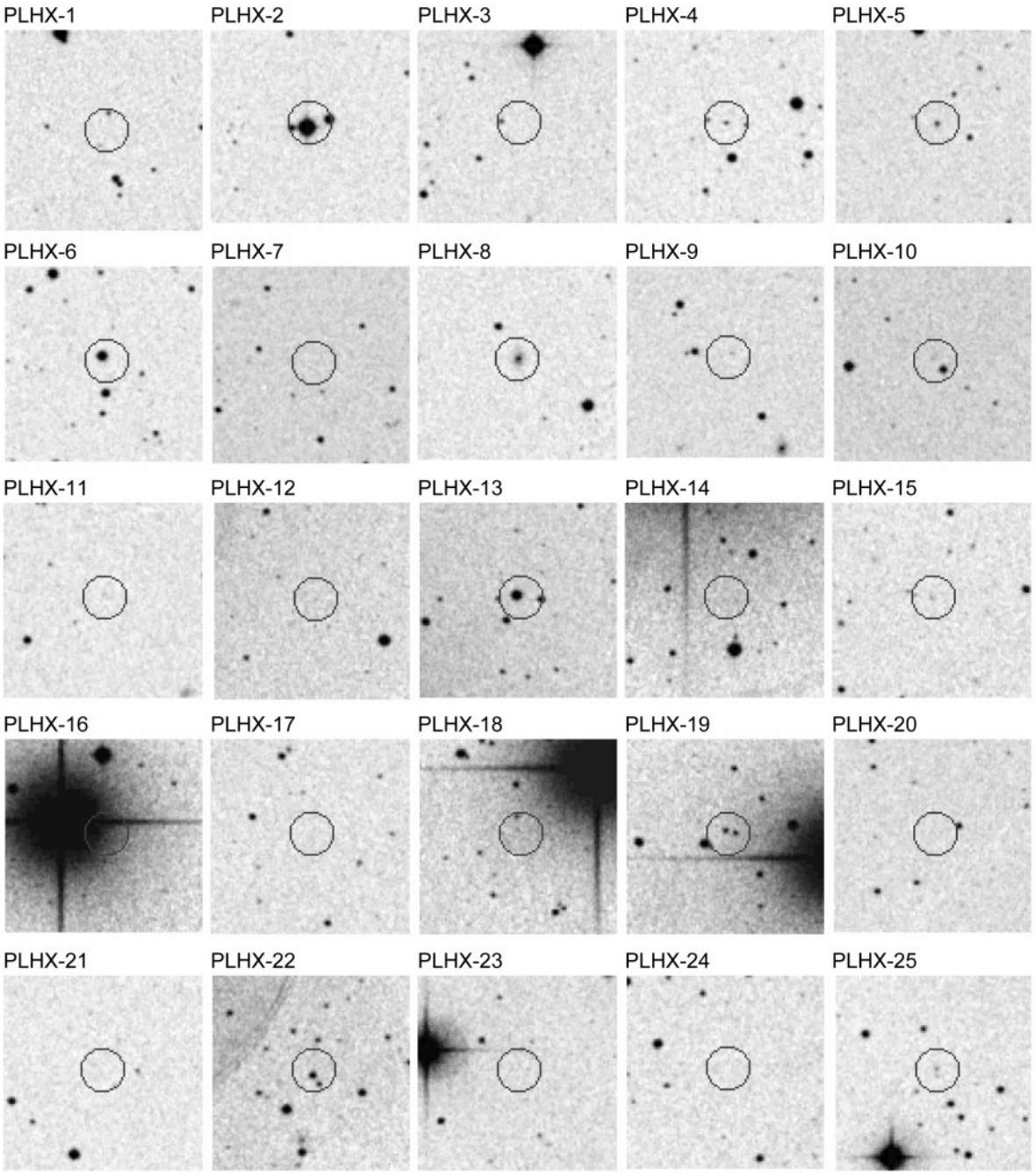

Fig. B1. Finding charts for unidentified HRI sources detected in the Pleiades region; star fields extracted from the STScI DSS. Each chart is 3' on a side, centered on the HRI position. Identification circles are indicated.

B.1. CCD photometry of unidentified sources

In regard to previous ROSAT PSPC and HRI observations in the Pleiades (Paper I and Paper II), CCD photometry of candidate optical counterparts for some unidentified X-ray sources has been obtained by one of us (CP). CCD photometry was obtained during 1992 November and 1994 November using a 2048^2 CCD on the 1.2m Whipple Observatory telescope at Mt. Hopkins, Arizona. During each night's observations, a set of extinction stars were monitored, along with standard stars taken from Landolt (1992) for the 1992 observations or with standards taken from Landolt (1992), Joner & Taylor (1990), and Schild (1983) for the 1994 observations. Each night's instrumental magnitudes were transformed onto a standard BV (Johnson) and I (Kron) system. Standards with Cousins-system V-I colors were transformed to the Kron V-I system using the transformation equations of Bessell & Weis (1987). The accuracy of the derived magnitudes is considered to be on the order of a few-several hundreths of a magnitude for the brighter ob-

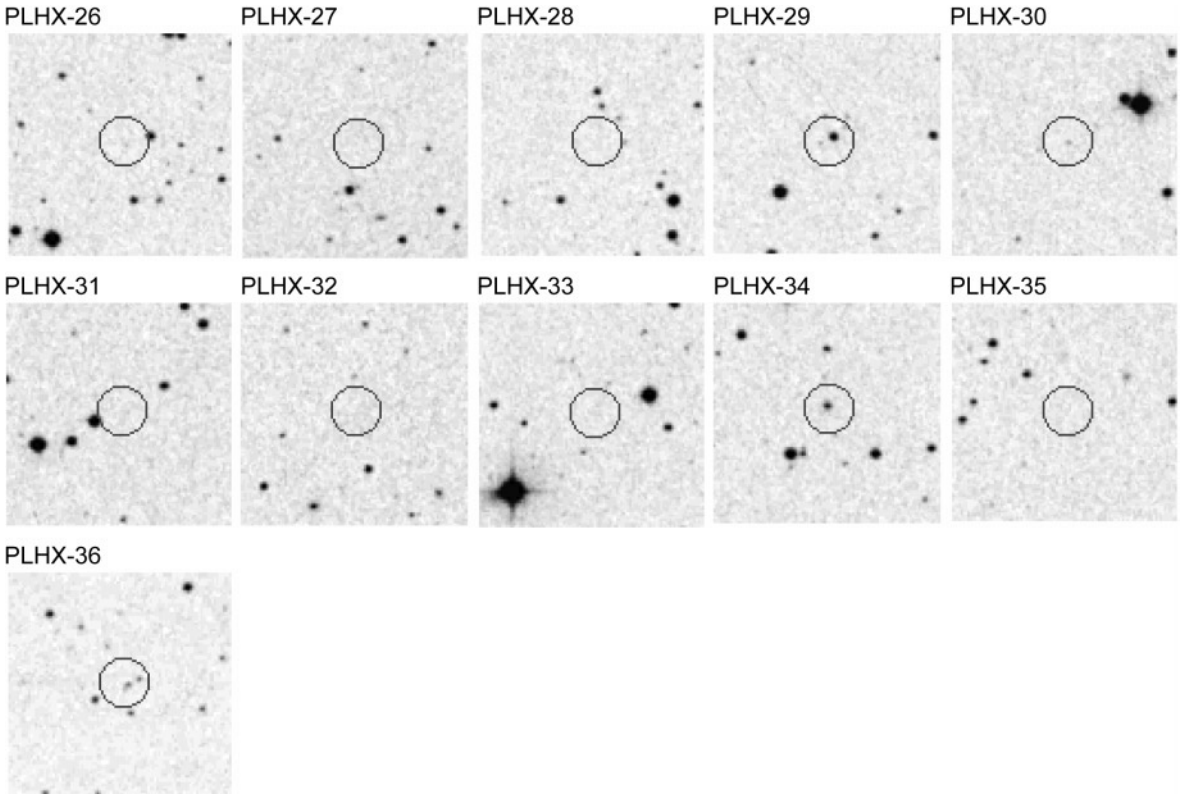

Fig. B1. (continued)

jects, increasing to on order 0.10 mag for the fainter objects measured.

In Table B2 we provide photometry for optical counterparts near the locations of unidentified PSPC X-ray sources from Paper I. These sources are identified by their source number from Paper I and given a prefix name "PLEX" for Pleiades X-ray source. The PLEX sources in Table B2 were all observed within the Northwest PSPC field of Paper I. In Table B2 we list source name, available VI photometry, the number of observations in each filter, and a flag indicating whether the object's photometry would be consistent with cluster membership. The final column provides additional notes, including relative locations of the optical counterparts on the finding charts in Fig. 8 of Paper I, and cross-references to optical star identifications and/or the PLHX X-ray sources detected in the present HRI observations. At the end of Table B2 are listed two additional X-ray sources which were not reported in Paper I, but which were detected in the standard analysis provided by the ROSAT Science Data Center with the original data. These sources have been sequentially numbered continuing from PLEX317 in Paper I While PLEX318 has been identified with the proper motion candidate member HHJ273 (Hambly et al. 1993), the optical counterpart to PLEX319 appears to be a red star with relatively large proper motion and is not considered at this time to be a cluster member, although its photometry would be consistent with cluster membership.

We list in Table B3 those PSPC sources originally listed as 'unidentified' from Table 6C of Paper II. We include in this table the source identified with the star HII-1403 since Paper II uncorrectly listed it among the non identified sources. The columns in Table B3 give 2000 coordinates, available BVI photometry, the number of observations in each filter, and a flag indicating whether the object's photometry would be consistent with cluster membership. The final column provides additional notes and/or cross-references, PLHX numbers refer to the HRI source number in Table B1, and PLEX number refers to the PSPC source number from Paper I. Due to a nearby bright star and extreme faintness of the optical counterparts for the source at (3:46:23.7, 23:55:39.4), reliable photometry could not be obtained from the available observations. Among the sources of Table B3, one corresponds to a non-member HII star and another, PLHX22, has an optical counterpart with photometry consistent with cluster membership.

Appendix C: CCD photometry of cataloged stars around unidentified sources

In Table C1, we list CCD photometry for various catalogued stars which happened to be available for measurement on the CCD fields observed for the X-ray sources in Tables B3 and B2. Most of these stars have not had CCD photometry available previously. Included as a matter of interest in Table C1 is an extremely faint, red object (Anon1) found on the CCD observations which might be considered a candidate cluster member based on its limited photometry, though it could easily reveal itself to be a proper motion nonmember such as PLEX319 and

Table B2. CCD Photometry of Unidentified Sources from Stauffer et al. 1994

Name	V	V-I_K	vi	Mem	Notes
PLEX3	18.15	0.67	11	N	PLHX4, extended/galaxy?
PLEX5	17.88	1.25	11	N	PLHX5, galaxy
PLEX15	19.77	1.37	22	N	PLHX9, galaxy?
PLEX17	11.42	0.75	11	Y	AK1B121: B-V= 0.83, V-Rk=0.42
PLEX21	17.32	0.75	11	N	brighter object to NW within circle
	18.72	0.68	11	N	fainter object to N within circle
	16.73	0.97	11	N	bright object to SE just outside circle
PLEX22	19.13	0.73	11	N	western object of pair north of X-ray position
	19.76	1.31	11	N	eastern object of pair north of X-ray position
	20.04	0.77	11	N	fainter object south of pair
PLEX23	21.09	1.43	11	N	faint object approx. 30arcsec S of X-ray position
PLEX27	20.29	1.19	22	N	
PLEX29	...	...	01		faint object 30arcsec south of HII150 has Ik $\simeq$ 18.5
PLEX45	20.52	2.05	11	N	galaxy?
PLEX52	21.77	2.67	11	N	object to NW of X-ray position
PLEX61	18.07	3.19	11	Y	HHJ-243
PLEX64	16.14	2.26	11	Y	HCG-156: B-V= 1.59, V-Rk=1.18
PLEX73	19.15	1.27	11	N	galaxy
PLEX76	17.90	1.00	22	N	star to SW of X-ray position on circle edge
	17.40	1.59	22	N	star to S of X-ray position on circle edge
PLEX77	19.88	0.77	11	N	faint object approx 50arcsec east of X-ray position
PLEX78	20.27	1.63	22	N	PLHX15
PLEX82	19.50	3.35	22	Y	HHJ-48
PLEX87	21.11	1.12	11	N	PLHX17
PLEX318	17.61	2.74	22	Y	HHJ-273, X-ray source at: 3:45:19.4, 24:32:20 (2000)
PLEX319	19.93	3.33	44	N	X-ray source at: 3:45:24.3, 24:38:53 (2000)

Notes: PLEX3: object to east of X-ray position has (V,V-Ik) = (18.22, 0.81); object to west of X-ray position has (V,V-Ik) = (18.52, 0.91)
PLEX15: brighter star to east, just outside circle on chart, has (V,V-Ik) = (16.25, 1.19)
PLEX23: brighter star to southwest, outside of circle has (V,V-Ik) = (15.80, 1.04)
PLEX45: brighter star on edge of circle to west has (V,V-Ik) = (16.62, 1.05)
PLEX73: another galaxy approx. 30arcsec W of PLEX73 has (V,V-Ik) = (18.95, 1.30)
PLEX76/77: these two "sources" lie near each other, may in fact be one source.

Table B3. CCD Photometry of unidentified Sources from Micela et al. 1996

RA (J2000)	DEC (J2000)	V	B-V	V-I_K	vbi	Mem	Notes
3:46:03.9	23:57:46.7	18.50	...	1.31	101	N	PLEX114
3:46:06.6	23:53:38.2	20.74	...	2.01	101	N	
3:46:23.7	23:55:39.4	...	...	...	...		(a)
3:47:09.3	24:03:06.5	16.63	...	2.48	101	Y	PLHX22
		17.59	...	1.16	101	N	
3:47:24.2	23:54:03.7	13.96	0.91	0.85	111	N	HII1403
3:47:39.1	23:33:56.6	18.81	...	1.17	101	N	PLHX25
		19.18	...	0.81	101	N	
3:48:07.2	24:16:34.0	17.41	1.13	1.09	111	N	

(a) there are two optical objects near the X-ray position

further observations would be necessary to ascertain its membership status. Comparison of the 1992 CCD images with the Digitized Sky Survey from STScI of a plate taken 1951 in fact suggests the possibility of detectable proper motion.

Table C1. CCD Photometry of Stars around nonidentified X-ray sources

Name	V	B-V	V-R_K	V-I_K	vbri	Mem
HII 81	13.56	0.94	0.52	0.86	1111	N
HII 83	14.83	1.13	0.62	1.02	1111	N
HII450	16.20	1.00	0.53	0.83	1111	N
SK-586	17.19	...	...	2.66	1001	Y
SK-676	16.50	...	...	2.44	1001	Y
SK-702	17.31	...	...	2.71	1001	Y
HCG-109	17.28	...	...	2.66	2002	Y
HCG-145	16.64	...	...	2.49	1001	Y
HCG-146	17.87	...	...	2.87	1001	Y
HCG-160	16.79	...	...	2.53	1001	Y
HCG-170	16.30	0.80	0.51	0.69	1111	N
HCG-177	16.87	...	...	2.56	1001	Y
HCG-181	16.14	...	...	2.36	1001	Y
HCG-194	16.69	...	...	2.79	3002	Y
Anon1	22.75	...	...	4.78	1001	Y?

Anon1: approx. optical position= 3:44:52.5, 24:36:52 (2000)

References

Barbera M., Micela G., Sciortino S., Harnden, F.R. Jr., Rosner R., 1993, ApJ 414, 846
Barbera M., Collura A., Dara, A., et al., 1997, ExpAstr 7, 51
Belloni T., Tagliaferri G., 1997, A&A 326, 608
Belloni T., Tagliaferri G., 1998, A&A 335, 517
Belloni T., Verbunt F., 1996, A&A 305, 806
Bessell M.S., Weis E.W., 1987, PASP 99, 642
Branduardi-Raymont G., Mason K.O., Warwick R.S., et al., 1994, MNRAS 270, 947
Briel U.G., Pfeffermann E., 1995, Proc. SPIE 2518, 120
Caillault J.-P., Helfand D.J., 1985, ApJ 289, 279
Cattaneo F., Hughes D.W., 1996, Phys. Rev. E 54, 4532
Dachs J., Hummel W., 1996, A&A 312, 818
Damiani F., Maggio A., Micela G., Sciortino S., 1997, ApJ 483, 370
David L.P., Harnden F.R. Jr., Kearns K.E., Zombeck M.V., 1993, The Rosat High Resolution Imager (HRI). U.S. ROSAT Science Data Center/Sao
Favata F., Micela G., Sciortino S., Vaiana G.S., 1992, A&A 256, 86
Gagné M., Caillault J.-P., Stauffer J.R., 1995, ApJ 450, 217
Giampapa M.S., Prosser C.F., Fleming T.A., 1998, ApJ, in press
Hambly N.C., Hawkins M.R.S., Jameson R.F., 1993, A&AS 100, 607
Hasinger G., Burg R., Giacconi R., et al., 1993, A&A 275, 1
Hertzsprung E., 1947, Ann. Leiden Obs. 19, Part 1A
James D.J., Jeffries R.D., 1997, MNRAS 292, 252
Jeffries R.D., Thurston M.R., Pye J., 1997, MNRAS 287, 350
Johnson H., 1966, ARA&A 4, 190
Joner M.D., Taylor B.S., 1990, PASP 102, 1004
Jones B.F., Fischer D.A., Stauffer J.R., 1996, AJ 112, 1562
Krishnamurthi A., Terndrup D.M., Pinsonneault M.H., et al., 1998, ApJ 493, 914
Landolt A., 1992, AJ 104, 340
Lang K.R., 1992, Astrophysical Data: Planets and Stars. Springer, New York
Maggio A., Sciortino S., Vaiana G.S., et al., 1987, ApJ 315, 687
Mermilliod J.-C., Turon C., Robichon N., Arenou F., Lebreton Y., 1997, In: Perryman M.A.C., Bernacca P.L. (eds.) Hipparcos Venice '97. 643
Micela G., Sciortino S., Serio S., et al., 1985, ApJ 292, 172
Micela G., Sciortino S., Vaiana G.S., et al., 1990, ApJ 348, 557
Micela G., Sciortino S., Favata F., 1993, ApJ 618, 412
Micela G., Sciortino S., Kashyap V., Harnden F.R. Jr., Rosner R., 1996, ApJS 102, 75
Monet D., Dahn C., Vrba F., et al., 1992, AJ 103, 638
Noyes R.W., Hartmann L.W., Baliunas S.L., Duncan D.K., Vaughan A.H., 1984, ApJ 279, 763
Pallavicini R., Golub L., Rosner R., et al., 1981, ApJ 248, 279
Patten B.M., Simon T., 1993, ApJ 415, L23
Patten B.M., Simon T., 1996, ApJS 106, 489
Prosser C.F., Randich S., 1997, Center for Astrophysics Preprint No 4537
Prosser C.F., Schild R.E., Stauffer J.R., Jones B.F., 1993a, PASP 105, 269
Prosser C.F., Shetrone M.D., Marilli E., et al., 1993b, PASP 105, 1407
Prosser C.F., Stauffer J.R., Caillault J.-P., et al., 1995a, AJ 110, 1229
Prosser C.F., Shetrone M.D., Dasgupta A., et al., 1995b, PASP 107, 211
Prosser C.F., Randich S., Stauffer J.R., Schmitt J.H.M.M., Simon T., 1996, AJ 112, 1570
Prosser C.F., Randich S., Simon T., 1997, Center for Astrophysics Preprint No 4538
Pye J.P., Hodgkin S.T., Stern R.A., Stauffer J.R., 1994, MNRAS 266, 798
Queloz D., Allain, S., Mermilliod, J.-C., Bouvier, J., Mayor, M., 1998, A&A, in press
Randich S., Schmitt J.H.M.M., 1995, A&A 298, 115
Randich S., Schmitt J.H.M.M., Prosser C.F., Stauffer J.R., 1995, A&A 300, 134
Randich S., Schmitt J.H.M.M., Stauffer J.R., Prosser C.F., 1996a, A&A 305, 785
Randich S., Schmitt J.H.M.M., Prosser C., 1996b, A&A 313, 815
Rucinsky S.M., 1984, A&A 132, L9
Schild R.E., 1983, PASP 95, 1021
Schmitt J.H.M.M., Kahabka P., Stauffer J.R., Piters A.J.M., 1993, A&A 277, 114
Sciortino S., Micela G., Favata F., 1995, A&A 296, 370
Simon T., Patten B.M., 1998, PASP 110, 283
Snowden S.L., 1998, ApJS 117, 233
Snowden S.L., McCammon D., Burrows D.N., Mendenhall J.A., 1994, ApJ 424, 714
Stark A.A., Gammie C.F., Wilson R.W., et al., 1992, ApJS 79, 77
Stauffer J., Hartmann L., 1987, ApJ 318, 337
Stauffer J., Klemola A., Prosser C., Probst R., 1991, AJ 101, 980
Stauffer J.R., Caillault J.-P., Gagné M., Prosser C.F., Hartman L.W., 1994, ApJS 91, 625
Stern R., Schmitt J.H.M.M., Rosso C., et al., ApJL 1992, 399, L159
Stern R., Schmitt J.H.M.M., Rosso C., et al., 1994, ApJ 427, 808
Vainshtein S., Sagdeev R., Rosner R., 1997, Phys. Rev. E 56(2), 1605-22
Zombeck M.V., Conroy M., Harnden F.R. Jr., et al., 1990, Proceedings of the SPIE Conference on EUV, X-Ray and Gamma-Ray Instrumentation for Astronomy 1344, 267
Zombeck M.V., Barbera M., Collura A., Murray S.S., 1997, ApJL 487, 69